Chemical routes to materials



Block copolymer templated synthesis of mesoporous WO₃/carbon nanocomposites

John Bentley¹ and Bishnu Prasad Bastakoti^{1,*}

¹ Department of Chemistry, North Carolina A & T State University, 1601 E Market St, Greensboro, NC 27411, USA

Received: 1 April 2022 Accepted: 16 July 2022 Published online: 3 August 2022

This is a U.S. Government work and not under copyright protection in the US; foreign copyright protection may apply 2022

ABSTRACT

We synthesize mesoporous WO_3 /carbon composites with PS-PVP-PEO polymeric template. The molecularly dissolved polymer in THF self-assembles in positively charged spherical micelles upon the addition of HCl. The negatively charged tungsten source (WO_4^{2-}) binds strongly with positively charged polymeric micelles. Glucose, WO_4^{2-} , and micelles are assembled as a mesostructure during solvent evaporation. The carbonization of composites leads to mesoporous WO_3 /carbon nanocomposites. A polymeric micelle having unique blocks for porogen (polystyrene), reaction site (polyvinyl pyridine), and stabilizer (ethylene oxide) makes the system exceptional to synthesize mesoporous nanocomposites in a one-pot method. The nanocomposites were characterized by dynamic light scattering, scanning electron microscopy, transmission electron microscopy, Fourier transforms infrared spectroscopy, X-ray photoelectron spectroscopy, and Raman spectroscopy. The electrochemical studies reveal that the composites deliver 381 F.g $^{-1}$ capacitance with 96% retention in 1 M H $_2$ SO $_4$.

Introduction

Template-assisted synthesis is a method where low molecular surfactants or amphiphilic block copolymers are used as templates and structure-directing agents [1]. It allows for more control over the synthesis route giving the ability to interchange different polymer blocks for desired functions or size. This synthetic approach's simplicity, flexibility, and reproducibility allow the fabrication of several mesoporous inorganic materials [2]. The inorganic

sources interact with the hydrophilic portion, whereas the hydrophobic part of amphiphilic diblock copolymer templates for getting a porous structure [3]. Polystyrene-polyethylene oxide diblock copolymer was used to synthesize mesoporous carbon-WO₃ and carbon via evaporation induced self-assembly (EISA) method [4]. The addition of PS homopolymers in the solubilizing process led to larger mesopores [5]. The PEO-based block copolymers with hydrophobic blocks such as polypropylene oxide, polystyrene, polymethyl acrylate, polybutylene have

Handling Editor: Dale Huber.

Address correspondence to E-mail: bpbastakoti@ncat.edu



been frequently studied to get a broader range of porous inorganic materials [6–9]. In the EISA process, block copolymers and inorganic sources undergo closely-packed structures with appropriate packing parameters. The packing parameter depends on the hydrophobic-hydrophilic ratio of the block copolymer, polymer-inorganic source ratio, and solution properties such as solvent compositions [10]. Mesoporous structures with spherical or cylindrical, bicontinuous, or gyroid pores are obtained after removing the template by solvent extraction or calcination [6].

The addition of the third reactive block on the diblock copolymer adds up the simplicity and generality of the method [11]. A laboratory synthesized triblock copolymer (PS-AAA-PEO) with core-shellcorona micelles was used to fabricate mesoporous nickel ferrite [12]. The strong interaction of acrylic acid and metal ions and the high thermal stability of polymer is another advantage towards obtaining crystalline mesoporous materials having lower crystallization temperature through calcination at higher temperatures [13]. The hydrophobic PS with higher glass transition temperature forms a rigid core in an aqueous based solution which stabilizes the micelles and controls the pore size of mesoporous materials. The switching of the reactive blocks widens its interaction with inorganic sources. Nakashima et al. synthesized several porous hollow structures using PS-PVP-PEO block copolymer [14]. The use of polyvinyl pyridine shells as reaction sites makes the synthetic method easy with strong interaction of negatively charged inorganic sources such as PtCl₄²⁻, WO_4^{2-} , MO_4^{2-} , and SnO_3^{2-} . The reactive block of copolymer strongly interacts with inorganic sources enabling the fabrication of a highly robust framework. The hydrophilic PEO helps orderly packing of the micelles during solvent evaporation. The pore sizes and wall thicknesses can be easily tuned to several nanometers by varying the block lengths of hydrophobic and metal source concentrations, respectively [14]. Mesoporous TiO₂, Nb₂O₅, WO₃, SnO₂, SiO₂, Al₂O₃, and ZnO are synthesized using different triblock copolymers [6, 14, 15].

Tungsten oxide has excellent properties to be applied as pseudocapacitive electrode material being an n-type semiconducting transition metal oxide with multiple crystal phases, and high conductivity [16]. It contains electron holes that act as charge traps which we believe will help with storage capacity. It has a

wide and stable band gap, and when tuned, it affects optical properties providing the potential to develop a transparent supercapacitor with high theoretical capacitance [17]. The reversible redox reaction between W⁵⁺ and W⁶⁺ ions makes the WO₃ noteworthy metal oxides in battery and supercapacitor applications. The intrinsic void on the crystal structure eases the diffusion of the ions from the electrolytes [18]. Previous studies have shown that the nanostructured WO₃-based materials with controlled crystallinity, morphology, pore size, and specific surface area are beneficial for improving the specific capacitance, energy and power density [19, 20]. However, WO₃ is challenged with overcoming the drawbacks of poor electrical conductivity and lower cycling ability. Combining other materials, predominantly electrostatic double-layer capacitors type materials such as carbon, graphene, and carbon nanotubes with WO₃ is an effective way to enhance the supercapacitance.

Biomass activated carbon-decorated WO_3 nanocomposites were synthesized through a sonochemical method. The bulk WO₃ was broken into flakes and mixed with activated carbon. The composites showed promising electrocatalytic activities for oxygen and hydrogen evolution reaction with relatively lower overpotential in alkaline solution [21]. The porous MnO₂-carbon composite retained its high specific surface area, which was higher than either bare mesoporous carbon or MnO2 electrode materials. The performance was better than that of MnO₂ prepared with a carbon nanotube template under the same conditions [22]. Tungsten oxide containing nitrogen-doped-graphene quantum dots possessed excellent cyclic stability with a high specific capacitance of 178.82 Fg^{-1} [23]. Ln_2O_3 nanoparticles were successfully incorporated into the mesoporous carbon framework by an impregnated method. The mesoporous framework was synthesized using the complicated templating process. The multiple steps take more human effort and loss the intermediate products during synthesis [24]. The onepot synthesis method overcomes the shortcomings of multistep synthesis.

Here, we have synthesized mesoporous tungsten oxide–carbon composites via micelles assembly using a PS-PVP-PEO template in a single pot method. WO₃ nanoparticles are firmly anchored on the mesoporous carbon framework (Scheme 1). The composites are well characterized using several tools and techniques



such as scanning electron microscope (SEM), Transmission electron microscope (TEM), Fourier transform infrared (FTIR) spectroscopy, Raman spectroscopy, and X-ray photoelectron spectroscopy (XPS). The electrochemical properties are studied using cyclic voltammetry measurements from a three-electrode system. The uniformly distributed WO₃ nanoparticles through the carbon mesostructured are effectively utilized to enhance capacitive performances. Through a combination of both faradaic and non-faradaic processes, WO₃-mesoporous carbon exhibited a high specific supercapacitance of 381 F.g⁻¹ in 1 M H₂SO₄.

Experimental

Materials

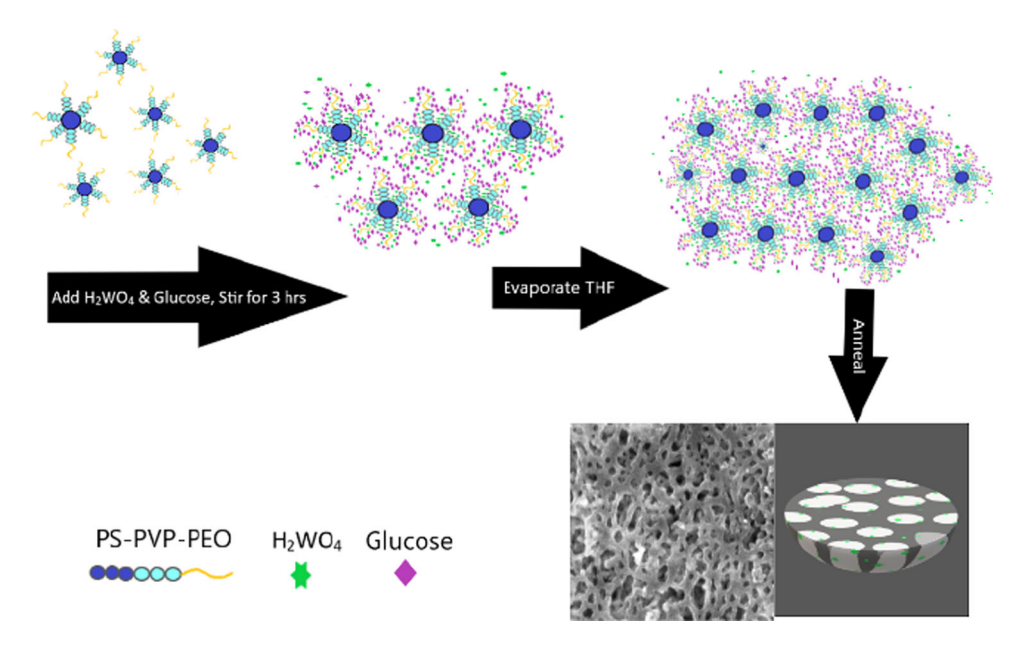
Poly(styrene-*b*-2-vinyl pyridine-*b*-ethylene oxide) PS(14,500)-*b*-P2VP(20,000)-*b*-PEO(33,000) (Polymer Source. Inc.), Tungstic (VI) acid (H₂WO₄; Alfa Aesar), D-(+)-Glucose (Sigma-Aldrich), tetrahydrofuran (THF; Fisher Chemical), hydrochloric acid (HCl; Fisher Chemical), Sulfuric acid (H₂SO₄; Fisher Chemical), and Naflon D-521 (Alfa Aesar) were used without further purification.

Methods

Porous nanocomposites consisting of WO₃ and carbon support were synthesized via micelles assembly

Scheme 1 Synthesis of mesoporous WO3/C composites via micelles assembly.

approach by dissolving 50 mg of PS-PVP-PEO block copolymer in 10 mL of tetrahydrofuran via sonication for 30 min. 80µL hydrochloric acid was added to the clear solution and was stirred for two hours. Then 40 mg of glucose dissolved in 200μL of DI water, and 40 mg of H₂WO₄ dissolved in 200μL ethanol was added into polymer solutions. The size and zeta potential of dissolved micelles were collected before and after adding tungstic acid by dynamic light scattering using a Malvern Zetasizer. After stirring for three hours, solutions were transferred to a petri dish to dry at room temperature. The dried sample was kept at 100 °C for 2 h and calcined at 600 °C for three hours with a ramping rate of 1 °C per minute in a nitrogen environment. Infrared spectroscopy of each sample before and after calcination was collected using the attenuated total reflection method. Horiba Raman spectroscopy and Thermo Scientific Escalab X-ray photoelectron spectrometer were used to analyze the chemical compositions of the sample. The morphology was observed by scanning electron microscope (ZEISS EVO-LS10) and transmission electron microscope (TEM; JEOL JEM-1210). The CH Instruments electrochemical workstation was used to study the electrochemical properties using a threeelectrode system. The working electrode was prepared by casting WO₃/carbon nanocomposites dispersed in water on a glassy carbon electrode. The casting solution was prepared by dispersing 5 mg of WO₃/carbon nanocomposites in 1 mL of deionized water, dropping 10 µm onto the glassy area of the





electrode. Once dried, then $5\mu L$ of Nafion solution was added over the sample, allowing it to dry. A platinum wire was used as the counter electrode and a saturated Ag/AgCl electrode as the reference electrode in 1 M H_2SO_4 solution.

Results and discussion

We synthesized mesoporous WO₃/carbon composites using a micelle assembly templating method. The uniqueness of our synthesis is the micelles we use and the matter of which they introduce the metal source into the self-assembly. The polymer, poly (styrene-b-2-vinyl pyridine-ethylene oxide) forms spherical micelles with PS core, PVP shell, and PEO corona in THF adjusted with HCl [25]. The molecularly dissolved polymer in THF appears turbid upon the addition of HCl (Figure S1). This can be attributed to protonation caused by the addition of HCl which formed radicals and started the self-assembly of the micelles. This also turns PS to hydrophobic state and allows it to form hollow opening in the composite after calcination. At the same time, the PVP block (shell) is being prepared to create charge attraction with the metal source, which in return is responsible for the placement of WO₄²⁻ ions on the pores' surface. The HCl protonates the nitrogen on the PVP's pyridine ring. In the stirring phase of the synthesis, these positively charged nitrogen draws attraction to the negatively charged WO₄²⁻ ions and attach to the micelle. The PEO block of the micelle serves as a structure directing agent that aids in the self-assembly of the composite.

The first vital step to deem our synthesis successful is the attachment of the WO_4^{2-} ions on the template. To ensure the WO_4^{2-} is attached to the template, we study the hydrodynamic diameter (DLS) and zeta potential of polymeric before and after adding WO_4^{2-} ions. When WO_4^{2-} is added, average size increases from 108 to 994 nm diameter. Multiple bands on the DLS profile show the formation of multiaggregates of WO₄²⁻/micelles composites (Figure S2). The increase in diameter is due to the intermicelles aggregations. We observed an increase in size and a decrease in the zeta potential; the positively charged (+ 28 mV) micelles show - 3.20 mV zeta potential after loading WO_4^{2-} . The zeta potential is the potential difference between the dispersion medium and the surface of nanoaggregates, and it is

caused by the net electrical charge contained within the region bounded by the slipping plane. The magnitude of the zeta potential indicates total surface charge and degree of electrostatic repulsion among the nanoaggregates. As the solution dries, the micelles form an affinity, resulting in a single framework (Scheme 1). The sample is annealed at 600 °C for 3 h with a 1 °C/min ramping rate in nitrogen crystalized the WO₃ and carbonized glucose to form mesoporous WO₃/carbon nanocomposites.

FTIR spectra of pure polymer, polymer/WO₄²⁻/ glucose nanocomposites, and WO₃/carbon were taken (Fig. 1). The slight shift on the stretching peak of pyridine at 1590 cm⁻¹ indicates the strong interaction of WO₄²⁻ ions with polymer. FTIR of composites before and after calcination indicated complete removal/carbonization of the organic moieties. All peaks that had reference to the template present in the as-prepared sample were no longer present in the calcined samples. By carbonizing in nitrogen, our sample was able to maintain the carbon content as the template is broken down. As expected, when investigating the Raman data (Fig. 2), the composites containing tungsten showed peaks. There were two peaks at 272 and 324 cm⁻¹ for WO₃ composite with carbon and 256 and 372 cm⁻¹ for the WO₃ alone, and these peaks represent the W⁶⁺-O-W⁶⁺ bending vibration mode of bridging oxygen in the WO₃ crystal lattice. The peaks observed at 715 and 806 cm⁻¹, and 694 and 805 cm⁻¹ indicate the presence of the long and short W⁶⁺-O-W⁶⁺ bond

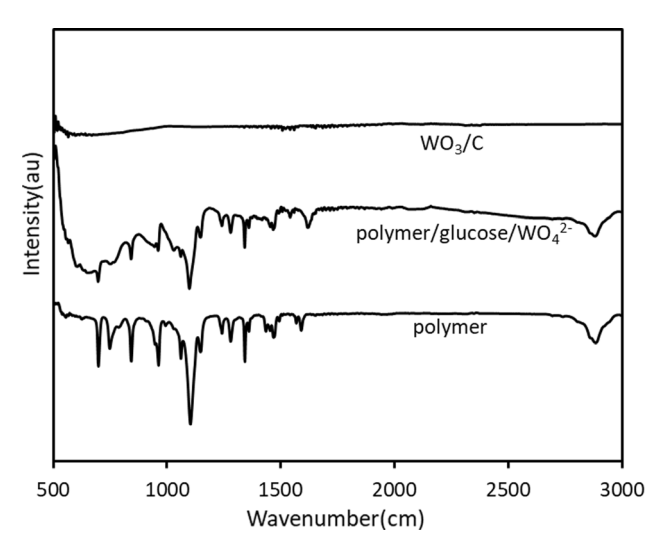


Figure 1 FTIR spectra of polymer, polymer/glucose/ WO_4^{2-} and WO_3 /carbon.



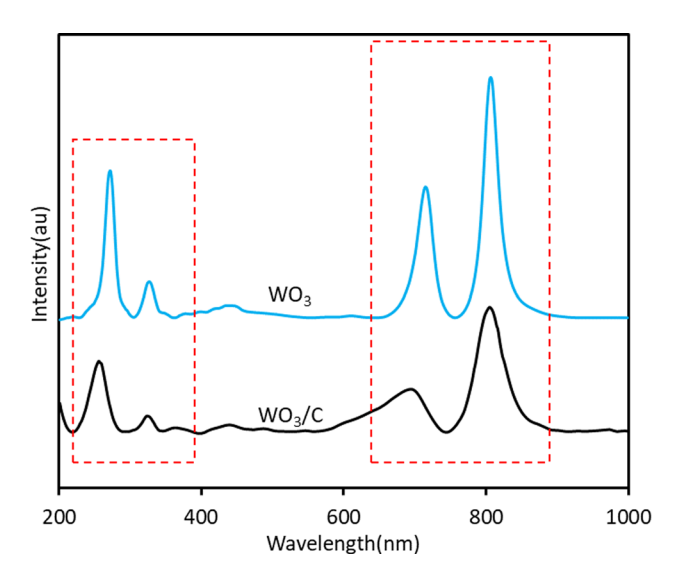


Figure 2 Raman spectra of WO₃ and WO₃/carbon.

stretching mode [26]. These shifts are caused by the presence of carbon. Using x-ray photoelectron spectroscopy, we were able to detect the binding energy of C 1, O 1 s, and W 4f for WO₃/carbon composites. Figure S3 shows the high-resolution XPS spectra of WO₃/carbon composites. The two peaks at 34.9 and 37 eV represents the spin–orbit splitting of the W $4f_{5/2}$ and W $4f_{7/2}$. 284 eV peak is due to the presence of elemental carbon. The CHN analysis reveals that 31% of carbon was present in the composites. The peaks of O 1 s are located at 529.8 and 531.0 eV, corresponding to C–O/W–O, and C–O, respectively [27].

The surface structure of polymer micelles and porous nanocomposites were observed under SEM (Fig. 3). The porous framework of carbon is observed. Very few WO₃ nanoparticles were seen on the outer surface. The TEM observation clearly showed that the WO₃ nanoparticles are firmly anchored on the framework. The TEM images show the distribution of WO₃ nanoparticles over the framework (Fig. 3c-d and Figure S4). The nanocomposites have a mesoporous structure with a pore size 30–40 nm. It is also confirmed by N₂ adsorption–desorption measurement. BET plot in the Fig. 4 shows that the composites have a high surface area of 78 m².g⁻¹ with a pore diameter around 40 nm.

A three-electrode system studied the electrochemical properties of WO_3 /carbon by cyclic voltammetry (CV). The CV is a reliable technique for the determination of redox potentials and electron-transfer redox reactions involved. The well-dispersed solution was put on the glassy carbon electrode and

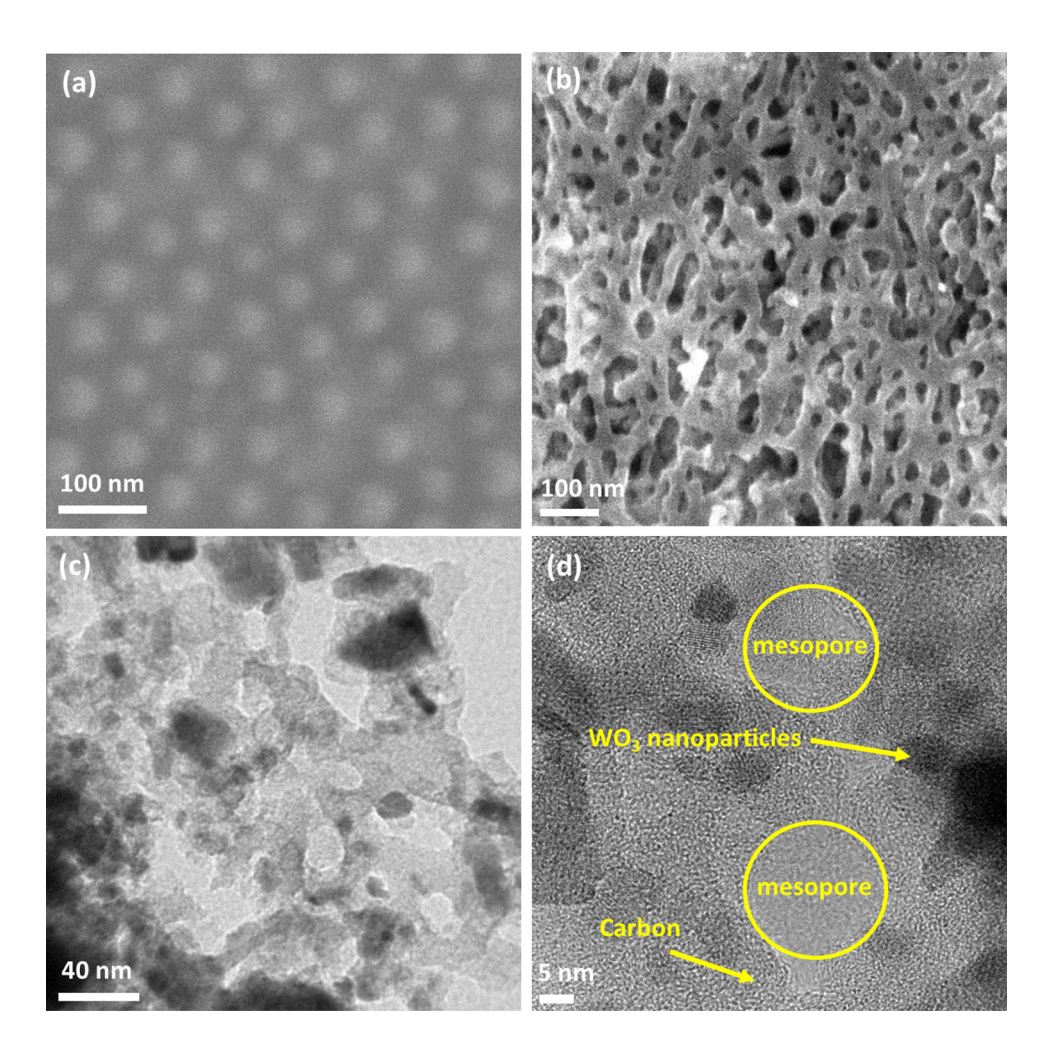
Nafion solution (0.5%) was used as a binder. The reversible redox reaction on the WO₃ electrode takes place between W⁺⁵ ions and W⁺⁶ ions. The following mechanism is an example of the cycle of exchanging the H⁺ ion between the surface of the WO₃/carbon nanocomposite and the electrolyte $(HxWO_3 \leftrightarrow$ $WO_3 + xH^+ + xe^-$) [28]. Typical CV curves at different scan rates obtained at room temperature are shown in Fig. 5. The nanocomposites are able to deliver a specific capacity of 381 F.g⁻¹ at scan rates of 5 mVs⁻¹ in 1 M H₂SO₄ solution. This is comparable with other published reports [29-31]. WO₃ and carbon synthesized using the same method are tested as electrode materials for comparison. Their performance is $(WO_3; 76 \text{ F.g}^{-1} \text{ and carbon}; 22 \text{ F.g}^{-1} \text{ at the})$ scan rate of 5 mV/s) lower than the WO₃/carbon nanocomposites. The combination of faradaic and non-faradaic processes makes the composites better electrode materials than the individual components. As shown in Figure S5, there is a decrease in specific supercapacitance as the scan rate increases. It happens because at faster scan rates electrolytes (ions) are only exchanged on the outer surface of the composite, whereas with slower scan rates the ions are exchanged on the surface of the pore walls deeper within the composite, which results in a higher supercapacitance value. The stability of samples was also tested over 1000 cycles at a scan rate of 50 mV/s. All samples showed to maintain above 96% retention of supercapacitance over the 1000 cycles indicating highly durable electrode materials for supercapacitors (Figure S6).

Conclusions

Mesoporous tungsten oxide carbon composites were developed using a PS-PVP-PEO template through micelle assembly. The protonation of the PVP block (shell) is used to create charge attraction with the metal source, which in return is responsible for the placement of WO₄²⁻ on the pores' surface. In the stirring phase of the synthesis, the positively charged nitrogen on the PVP's pyridine ring draws attraction to the negatively charged WO₄²⁻ and attaches to the micelle. We were able to identify attraction between the template and tungsten precursor by studying the zeta potential and noticing change before and after the addition of tungsten. Calcination of the materials resulted in voids being left in place of the carbonized



Figure 3 SEM image of a polymeric micelles. SEM b and TEM c-d images of WO₃/carbon nanocomposites.



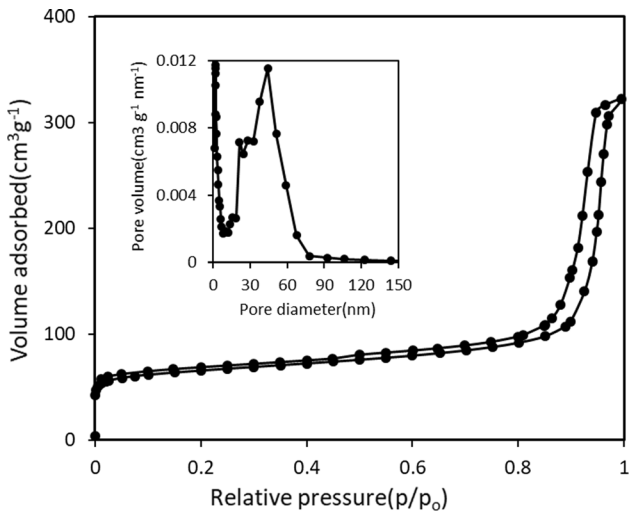


Figure 4 BET plot of WO₃/carbon nanocomposites. The inset shows the pore size distribution.

template. The addition of glucose acted as an additional carbon source. When reviewing the Raman

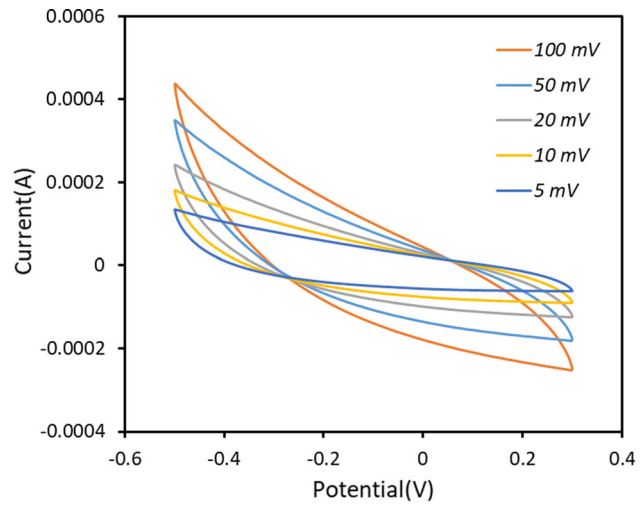


Figure 5 CV curves of WO₃/carbon at different scan rates.

data, there was a noticeable shift between composites prepared with glucose and those that were not, the W⁶⁺-O-W⁶⁺ bending vibration mode of bridging oxygen in the WO₃ crystal lattice, the presence of the



long and short W⁶⁺-O-W⁶⁺ bond stretching mode was caused by the presence of the additional carbon. When testing the nanocomposites' electrochemical properties, the cyclic voltammetry curves were stable, indicating reversible and fast redox surfaces at a constant rate. We were able to get a specific supercapacitance value of 381 F.g⁻¹. We tested capacitance over 1000 cycles with a retention of 96% capacitance. Given our composites' capacitance ability and cycle stability, it makes a great candidate for a supercapacitor electrode and helps combat the demand for the world's energy need.

Acknowledgements

B.P.B. thanks the National Science Foundation Research Initiation Award (2000310), Excellence in Research Award (2100710), USA, Joint School of Nanoscience and Nanoengineering, a member of the Southeastern Nanotechnology Infrastructure Corridor and National Nanotechnology Coordinated Infrastructure, which is supported by the National Science Foundation (Grant ECCS-1542174).

Declarations

Conflicts of interest There are no conflicts to declare.

Supplementary Information: The online version contains supplementary material available at https://doi.org/10.1007/s10853-022-07564-3.

References

- [1] Ariga K, Vinu A, Yamauchi Y, Ji Q, Hill JP (2012) Nanoarchitectonics for Mesoporous materials. Bull Chem Soc Jpn 85:1–32. https://doi.org/10.1246/bcsj.20110162
- [2] Bentley J, Desai S, Bastakoti BP (2021) Porous Tungsten oxide: recent advances in design, synthesis, and applications. Chem Eur J 27:9241–9252. https://doi.org/10.1002/chem. 202100649
- [3] Kannaiyan D et al (2010) Enhanced Photophysical properties of Nanopatterned Titania Nanodots/Nanowires upon Hybridization with Silica via block copolymer templated Sol-Gel process. Polymers 2:490–504. https://doi.org/10.33 90/polym2040490
- [4] Jo C et al (2013) Block-Copolymer-Assisted One-Pot synthesis of Ordered Mesoporous WO3-x/Carbon

- nanocomposites as high-rate-performance electrodes for Pseudocapacitors. Adv Funct Mater 23:3747–3754. https://doi.org/10.1002/adfm.201202682
- [5] Deng Y et al (2008) Ultra-Large-Pore Mesoporous carbons Templated from Poly(ethylene oxide)-b-Polystyrene Diblock Copolymer by Adding Polystyrene Homopolymer as a pore expander. Chem of Mater 20:7281–7286. https://doi.org/10. 1021/cm802413q
- [6] Li C et al (2020) Self-assembly of block copolymers towards mesoporous materials for energy storage and conversion systems. Chem Soc Rev 49:4681–4736. https://doi.org/10. 1039/D0CS00021C
- [7] Liu B et al (2015) Ligand-Assisted Co-Assembly approach toward mesoporous Hybrid Catalysts of Transition-Metal oxides and noble metals: photochemical water splitting. Angew Chem Inter Ed 54:9061–9065. https://doi.org/10.10 02/anie.201502892
- [8] Reitz C, Haetge J, Suchomski C, Brezesinski T (2013) Facile and general synthesis of thermally stable ordered Mesoporous Rare-earth oxide ceramic thin films with uniform mid-size to large-size pores and strong crystalline texture. Chem Mater 25:4633–4642. https://doi.org/10.1021/c m402995a
- [9] Liu Y et al (2018) A vesicle-aggregation-assembly approach to highly ordered mesoporous γ-alumina microspheres with shifted double-diamond networks. Chem Sci 9:7705–7714. h ttps://doi.org/10.1039/C8SC02967A
- [10] Zhao T, Elzatahry A, Li X, Zhao D (2019) Single-micelle-directed synthesis of mesoporous materials. Nat Rev Mater 4:775–791. https://doi.org/10.1038/s41578-019-0144-x
- [11] Olatidoye O, Thomas D, Bastakoti BP (2021) Facile synthesis of a mesoporous TiO2 film templated by a block copolymer for photocatalytic applications. New J Chem 45:15761–15766. https://doi.org/10.1039/D1NJ02997E
- [12] Tanaka S et al (2017) Self-assembly of polymeric micelles made of asymmetric polystyrene-b-Polyacrylic Acid-b-Polyethylene Oxide for the Synthesis of Mesoporous Nickel Ferrite. Eur J Inorg Chem 2017:1328–1332. https://doi.org/ 10.1002/ejic.201601459
- [13] Pizarro GDC et al (2019) Porous surface films with Tunable Morphologies and hydrophobic properties based on block copolymer under the effects of thermal annealing. Front Chem. https://doi.org/10.3389/fchem.2019.00181
- [14] Sasidharan M, Nakashima K (2014) Core–Shell–corona polymeric micelles as a versatile template for synthesis of inorganic hollow nanospheres. Acc Chem Res 47:157–167. https://doi.org/10.1021/ar4001026
- [15] Bastakoti BP, Li YQ, Kimura T, Yamauchi Y (2015) Asymmetric block copolymers for supramolecular



- templating of inorganic nanospace materials. Small 11:199-2–2002. https://doi.org/10.1002/smll.201402573
- [16] Santato C, Odziemkowski M, Ulmann M, Augustynski J (2001) Crystallographically oriented mesoporous WO3 films: synthesis, characterization, and applications. J Am Chem Soc 123:10639–10649. https://doi.org/10.1021/ja 011315x
- [17] Wu X, Yao S (2017) Flexible electrode materials based on WO3 nanotube bundles for high performance energy storage devices. Nano Energy 42:143–150. https://doi.org/10.1016/j. nanoen.2017.10.058
- [18] Yang H et al (2019) Structural, electronic, optical and lattice dynamic properties of the different WO3 phases: first-principle calculation. Vacuum 164:411–420. https://doi.org/10. 1016/j.vacuum.2019.03.053
- [19] Lokhande V, Lokhande A, Namkoong G, Kim JH, Ji T (2019) Charge storage in WO(3)polymorphs and their application as supercapacitor electrode material. Results Phys 12:2012–2020. https://doi.org/10.1016/j.rinp.2019.02. 012
- [20] Upadhyay KK et al (2017) On the supercapacitive behaviour of anodic porous WO3-based NEGATIVE ELECTRODES. Electrochim Acta 232:192–201. https://doi.org/10.1016/j.el ectacta.2017.02.131
- [21] Sekar S et al (2020) Enhanced water splitting performance of biomass activated carbon-anchored WO3 nanoflakes. App Surf Sci 508:145127. https://doi.org/10.1016/j.apsusc.2019. 145127
- [22] Wu D et al (2020) MnO2/Carbon composites for supercapacitor: synthesis and electrochemical performance. Front Mater. https://doi.org/10.3389/fmats.2020.00002
- [23] Sial QA, Javed MS, Lee YJ, Duy LT, Seo H (2020) Flexible and transparent graphene-based supercapacitors decorated with nanohybrid of tungsten oxide nanoflakes and nitrogendoped-graphene quantum dots. Ceram Int 46:23145–23154. https://doi.org/10.1016/j.ceramint.2020.06.094
- [24] Bastakoti BP et al (2013) Mesoporous carbon Incorporated with In2O3 nanoparticles as high-performance supercapacitors. Eur J Inorg Chem 2013:1109–1112. https://doi.org/10. 1002/ejic.201201311
- [25] Khanal A, Inoue Y, Yada M, Nakashima K (2007) Synthesis of Silica hollow nanoparticles Templated by Polymeric

- Micelle with Core-Shell-Corona structure. J Am Chem Soc 129:1534-1535. https://doi.org/10.1021/ja0684904
- [26] Gholami P, Khataee A, Bhatnagar A, Vahid B (2021) Synthesis of N-doped magnetic WO3–x@Mesoporous carbon using a diatom template and plasma modification: visible-light-Driven Photocatalytic activities. ACS Appl Mater Interfaces 13:13072–13086. https://doi.org/10.1021/acsami.0c21076
- [27] Kong W et al (2019) N doped carbon dot modified WO3 Nanoflakes for efficient photoelectrochemical water oxidation. Adv Mater Interfaces 6:1801653. https://doi.org/10.10 02/admi.201801653
- [28] Shinde PA et al (2017) Temperature dependent surface morphological modifications of hexagonal WO3 thin films for high performance supercapacitor application. Electrochim Acta 224:397–404. https://doi.org/10.1016/j.electac ta.2016.12.066
- [29] Ma L, Zhou X, Xu S, Zhang L, Ye C, Luo J, Chen W (2015) Hydrothermal preparation and supercapacitive performance of flower-like WO₃⋅H₂O/reduced graphene oxide composite. Colloids Surface A 481:609–615. https://doi.org/10.1016/j.c olsurfa.2015.06.040
- [30] Wang T, Liu H, Li J, Munir HA (2020) Facile preparation of h-WO₃/carbon cloth nanocomposite and its electrochemical properties for supercapacitors. ChemistrySelect 5:7704–7713. https://doi.org/10.1002/slct.202001733
- [31] Wen CY, Chen YC, Wang CM, Chen CH, Lin SY (2018) Composite electrodes of WO₃ coating on mesocarbon microbeads of a supercapacitor. Microsyst Technol 24:4049–4055. https://doi.org/10.1007/s00542-017-3618-z

Publisher's Note Springer Nature remains neutral with regard to jurisdictional claims in published maps and institutional affiliations.

Springer Nature or its licensor holds exclusive rights to this article under a publishing agreement with the author(s) or other rightsholder(s); author self-archiving of the accepted manuscript version of this article is solely governed by the terms of such publishing agreement and applicable law.

